Journal of the Brazilian Society of Mechanical Sciences and Engineering (2023) 45:384
https://doi.org/10.1007/s40430-023-04277-9

TECHNICAL PAPER

Investigation of tip leakage flow in spatial and temporal scales of axial isolated compressor rotor near stall

Hongwei Ma[1,2] · Zengzeng Wang[2] · Xiang He[1] · Yafei Zhong[2]

Received: 21 October 2022 / Accepted: 14 May 2023 / Published online: 29 June 2023

Abstract

To conduct detailed investigations about tip leakage flow in spatial and temporal scale at near stall, a total pressure probe, stereo particle image velocimetry (SPIV), dynamic pressure sensors array and validated numerical simulation are adopted at the near stall condition in a large scale iso-rotor compressor. Higher pressure regions are found propagating in circumference at near stall through different measurements technology. Completely different leakage vortex propagation characteristics are found assisted with SPIV technology at design and near stall condition, respectively. The rotor outlet total pressure dominant frequency shows an obviously non-synchronous characteristic, which is inconsistent with shaft frequency and blade pass frequency. The wall static pressure results and the vortex propagation frequency are also mutually confirmed nearly at 213 Hz. To investigate the propagation of pressure wave, an azimuthal mode analysis is adopted to get the spatial circular characteristic of disturbance. Furthermore, numerical results also show that the leakage vortex at near stall has propagated closer to the nearby blade pressure side, vortex broken position has advanced 10–20% chord length distance in the passage when compared with the design condition result. Rotating instability and the leakage vortex maintained a close association with the circulation propagation disturbance. Vortex line and blade frontal line intersection angle changed from 13° to 19° in a swing period.

Keywords Rotating instability · Axial compressor rotor · Tip leakage flow · Non-synchronous characteristic

List of symbols

Φ	Flow coefficient
Ψ	Static pressure rise coefficient

Subscripts

TLV	Tip leakage vortex
cps	Coefficient of static pressure
NSV	Non-synchronous vibration
SS	Suction surface
PS	Pressure surface
RI	Rotating instability
BPF	Blade pass frequency

Technical Editor: Daniel Onofre de Almeida Cruz, D.Sc.

✉ Hongwei Ma
mahw@buaa.edu.cn

[1] School of Energy and Power Engineering, Beihang University, Beijing 102206, China

[2] Research Institute of Aero-Engine, Beihang University, Beijing 102206, China

1 Introduction

The drive toward reduce engine weight and raise compress performance has pushed compressor stage loading increased, which caused a rise of non-synchronous vibration (NSV) near the stall boundary. The NSV generally contains many components at frequencies which are not integer multiples of shaft frequency and blade pass frequency (BPF) [1]. As today's research reveals, the non-synchronous vibration includes self-excited vibration and forced vibration components [2].

The NSV is a complex phenomenon that interact with multi-physics [3–8] as fluid, solid, acoustic, easily confused with other types of non-integral vibration. Extensive instruments and detailed numerical simulation are requested to distinguish the NSV. The unsteady flow propagated in the tip region is often called rotating instability (RI) which is also considered to have caused the forced vibration in NSV.

The NSV has received extensive attention since it was reported [9] in 1995. Experimental and numerical methods are capable tools to capture the vibration state [10–14] and obtain many valuable turbulent oscillation data and then develop the theory prediction tools [15–20]. The tip

clearance [21] between the rotor blade and casing wall has distinct influence on the leakage flow, which considered as a mainly reason for the NSV. The rotating speed [22] of the compressor have the same influence on the NSV as tip clearance. Due to tip clearance and rotating speed have a direct impact on tip flow as well as flow rates, tip leakage vortex becoming the hot research point. Tip leakage vortex will mix with the main flow in the blade passage, which induced flow instability and disturbance circumference propagation [23–26]. The unsteady tip flow with rotating rotor at different conditions derived many vibration forms. Alternation aerodynamic load act on the blade can cause blades fatigue even damage. The mechanisms of tip region flow oscillation and instabilities should be further researched and develop effective control method.

Casing wall pressure array [27, 28] and dynamic pressure probe [29] are often used to capture the tip flow unsteadies [30, 31]. The frequency spectrum analysis of the dynamic total pressure is a tool to distinguish the tip flow form. Casing wall pressure array [32] complete with stereo particle image velocimetry (SPIV) can help to capture the tip region passage flow characteristics. The azimuthal mode analysis [9, 33] is a tool to analyze the casing wall pressure to get the disturbance source number in the circular direction of the rotor. Numerical simulation has been utilized by researchers to analyze the rotating instabilities [34, 35] in tip region. The instability characteristic of tip leakage flow and vortex are intuitively analyzed with the simulation. Detailed propagation characteristic and spatial instability of the vortex are still need to be further clarified combined with experimental methods and numerical simulation.

Although the non-synchronous vibration of the compressor blade is considered as a multi-physics interaction problem, the aerodynamic instabilities problem in the blade tip region is still needs to further research, due to the aerodynamic disturbance occupied a leading role for the NSV. The tip leakage flow development in passages received less attention. Some researchers have found the vortex propagation in the circulation with SPIV and numerical simulation methods, discussed the relation with rotating instability and NSV [36, 37]. Some papers are focused on the phenomenon of propagation, but fewer papers focused on the detailed propagation and leakage vortex swing characteristics.

To clarify how the tip leakage flow influence on the no-integer multiples shaft frequency casing wall pressure and research the mechanism of rotating instability, an experimental test with casing wall pressure array and SPIV technology are executed. A numerical simulation based on the experimental near stall conditions are executed to get more valuable information from the tip region.

Though, the SPIV experiment can capture a leakage vortex propagation phenomenon in chordwise direction, limited by the SPIV system frequency, the blade passage result is time averaged. The slice section of SPIV is hard to place parallel to the casing wall to get the propagation in rotating direction. The propagation characteristic in the passage is hard to obtain from the experiment. The propagation characteristic is an important evidence for rotating instability. Therefore, numerical simulation method is utilized to obtain the passage propagated vortex and the rotating instability in multi-passages at the same moment. With the help of casing wall pressure sensors, dynamic single hole total pressure probe, SPIV technology and numerical simulation, data processing methods, the mechanisms of rotating instability and the non-synchronous aerodynamic characteristic are obtained in this paper.

2 Experimental setup

The experiment is developed in an isolated-rotor axial compressor in Beihang University (Fig. 1). The external diameter is 1 m, the hub ratio is 0.6. The blade profile is C4 low speed shape. The tip clearance size between the blade tip and the casing wall is 3 mm. More parameters of the compressor are shown in Table 1.

To reach the research objective of tip leakage flow induced rotating instability, casing wall pressure array, dynamic total pressure probe, five-hole probe and SPIV (stereo particle image velocimetry) are adopted to capture the tip and passage flow characteristic. The PXIe data acquisition platform and a phase locked trigger optical probe were utilized in the experiment. Calibration of the five-hole probe is performed in a low-speed wind tunnel. The five-holes pneumatic probe with 2 mm diameter head and 0.5 mm hole diameter is utilized to measure the radial flow parameters. The error of deflection angle and yaw angle are less than 0.3°. The total measurement error is less than 0.5%. The dynamic total pressure probe installed with SMI5882 piezoresistive pressure sensor is adopted to measure the rotor outlet flow. The Kulite dynamic pressure sensor is not selected for total pressure probe. The reason is that Kulite dynamic pressure sensor's minimum range is 5PSI (34.475 kPa). The maximum pressure arise of the isolated-rotor is 2 kPa, less than 6% of 5PSI. The

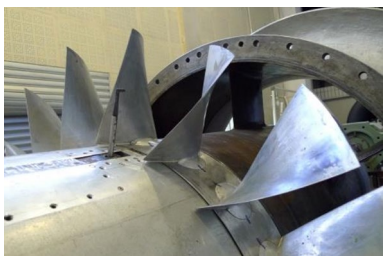

Fig. 1 Isolated-rotor experiment setup [30]

Table 1 Detailed list of the compressor key parameters

Name	Value
Casing diameter	1 m
Hub-casing-ratio	0.6
Rotor blade number	17
Chord length at tip	200 mm
Tip clearance size	3 mm (1.5%)
Design speed	1200 r/min
Design flow	22.4 kg/s
Reynolds number	$Re_{chord} = 7.5 \times 10^5$

Kulite dynamic pressure sensor has an amplitude error over the acceptable range. The maximum pressure measuring range of SMI5882 sensor is 0.6PSI. The dynamic calibration response frequency is 500 Hz. Two degrees of freedom (DOF) traverse mechanisms were utilized to control the probe motion and rotation. The traverse mechanism's linear displacement accuracy is less than 0.02 mm. The rotation angle error is less than 0.1°. The five-hole probe and the dynamic total pressure probe are installed in the casing wall as Pt probe as shown in Fig. 1. The PXIe data acquisition platform is set with 20 kHz sample rate and multichannel parallel acquisition.

To get the velocity field in the blade passage, advanced fluid velocity measurement technique stereo particle image velocimetry (SPIV) is adopted. The system is assembled by LaVision company. It contains two 12-bit 2048 × 2048 pixel Imager ProX4M CCD cameras, double cavity Nd:YAG laser(140 mJ/pulse), laser arm, PC, PTU, Davis software. The sample frequency is about 3-4 Hz. The average diameter of the tracing particles is around 1 μm. The cameras and laser are triggered by the phase locked part. The angle between two cameras is 60°, such as Fig. 2 shown. The blade with black tip which different from other blades is the locked signal trigger source. The SPIV window is placed at the horizontal direction position of the rotor as shown in Fig. 2.

The detailed measurements include the camera and the laser positions and the blade passage laser slice sections and the experimental error analysis were reported by Ma [30]. All test equipments are checked carefully. The maximum error of velocity measurement is less than 1.5% in the passage main flow, less than 6% in the tip region.

In this paper, measurements are mainly focused on the design condition and near stall condition, which flow coefficients equal to 0.65 and 0.55. In the chord direction, 14 dynamic pressure sensors are installed on the casing wall, as shown in Fig. 3.

The isolated-rotor compressor static pressure rise curves at different rotation speed are shown in Fig. 4. The compressor tip unsteady phenomenon at 900 RPM is similar to 1100 RPM, 700 RPM, so in this paper, all the measurements results are obtained at the reduced rotating speed $n_{cor} = 900$ RPM.

3 Numerical simulation procedure

To further research the unsteady leakage vortex in the tip region, numerical simulation is selected to reach this target. The numerical investigations are performed using the commercial codes ANSYS CFX for fluid calculations based on the isolated-rotor compressor in Beihang University, which mentioned in upon section. The unsteady simulation is obtained from the solver to get the tip leakage vortex motion in temporal scale. This part words are mainly record the calculation grids and the boundary conditions of the numerical simulation.

3.1 Calculation grids

The isolated-rotor compressor numerical grid models are shown in Fig. 5a and b. The computational domain of the inlet has been extended to 0.5 m and the outlet has been extended to 1 m. The commercial software ICEM is utilized to get hexahedra structure grids of the inlet and the outlet.

Four mesh grid strategies are simulated to get the static pressure rise coefficient at flow coefficient 0.61, aim to verify grid independence within the RANS frame, for which seven different numbers of grids are generated and listed in Table 2, and the corresponding results are illustrated in Fig. 5c.

The total number of the inlet and outlet mesh are 4.5million. The rotor grids are generated from TurboGrid with a HOH topology relationship. The rotor grids number is 4.15million. The y plus value from the simulation results is 17.

3.2 Unsteady simulation boundary conditions

In this solver, three-dimensional unsteady Reynolds averaged Navier–Stokes (URANS) equations are integrated in time by a fully implicit formulation of the second-order scheme for the compressible ideal gas with k-e turbulence model. The standard wall functions are used to deal with the near-wall flow. The rotation speed of this simulation is 900 RPM. The rotor and stator interface set as "Transient Rotor Stator", time step is 0.000196 s, which guaranteed 20 steps in one passage and total 10 revs simulation. The convergence criterion of the simulation is based on the residual level till to 1×10^{-6}. The axial intake inlet is set total pressure, 101325 pa with total temperature 288.15 K and turbulence degree 1.5%.

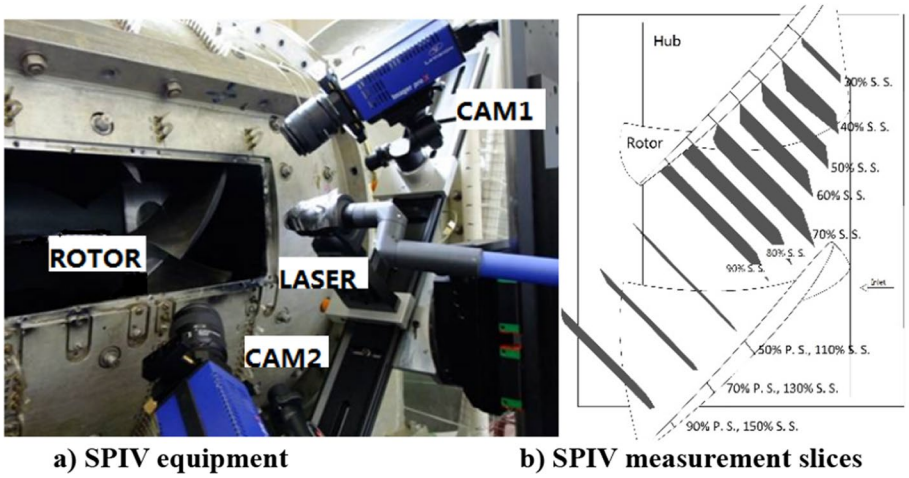

Fig. 2 Layout of SPIV experiment [30]

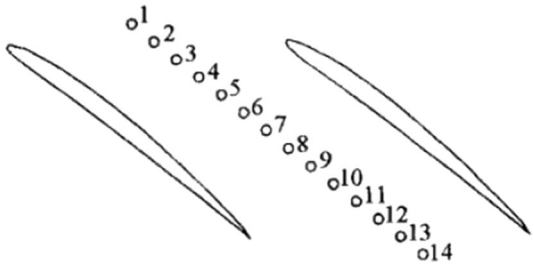

Fig. 3 Casing wall pressure sensors installation positions

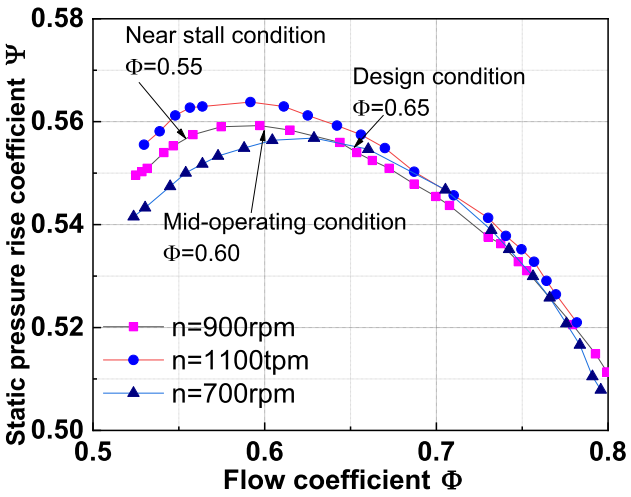

Fig. 4 Isolated-rotor compressor typical static pressure rise characteristic curve

3.3 Validation of numerical simulation

The aerodynamic performance curves of the isolated-rotor compressor from steady simulation and unsteady simulation are compared with the experimental curve as shown in Fig. 6. It is essential to notify that the experimental compressor has worked more than 20 years, blade has occurred some deformation, install angle has changed about 1° in 7 blades [38]. To verify the mesh resolution and the numerical model, a simulation with 7 blades non-uniform install angle steady and unsteady simulation have been conducted at 900 RPM, as shown with green triangle line. The non-uniform install angle simulation has a good uniformity with experimental data which labeled with magenta five-point star line. The uniform install angle simulation near stall point flow coefficient is 0.42, different with the experimental near stall flow coefficient point 0.55.

Besides, the boundary condition in simulation of inlet should be one of the reasons, numerical inlet is all absolute homogeneous and non-disturbance flow, but the inlet flow existence different scales turbulence in experiments which influenced by the experiment environment. The turbulence model k-e and the rotor- stator interface models are verified influence the predict precision. Non-uniformed install angle and variable tip clearance size make the rotor is more easily fall into the stall condition in experiment than the numerical simulation, which depict in Fig. 6. Though the non-uniform install angle steady and unsteady simulation has a better uniformity with the experimental, the non-uniform install angle may influence the tip flow circular propagation characteristic, a uniform install angle and equal tip clearance size at leading edge and trailing edge are selected as the basic model for this paper to analyze the rotating instability. In this paper, the simulation results are used to auxiliary understanding the tip leakage flow characteristic, no quantitative comparison between simulation and experiment has been mentioned.

The rotor outlet total pressure coefficients obtained from simulation and experimental are shown in Fig. 7, utilized to verify the numerical simulation model. Five-hole probe and total pressure probe and simulation results are compared in the span direction.

The total pressure probe results at the blade root position have a different trend compared with simulation and five-hole probe results. Main reason of this phenomenon is the total pressure probe's big head size and near-wall effect, hard to capture flow closer to the hub wall and introduced measurement error. At the near design point, Fig. 7a, the total pressure probe results have a good coincidence with the five-hole probe results in the span direction. With the decreased flow coefficients, the total pressure coefficients of total pressure probe are higher than the five-hole probe especially upon 50% span, this phenomenon is caused by the increased dynamic error of the total pressure probe at higher flow oscillation than the lower 50% span [39]. The simulation results at design point $\Phi = 0.65$ are coincided well with the experiment. The uniformity of the simulation and experiment is not good at flow coefficient $\Phi = 0.60$ and $\Phi = 0.55$ in Fig. 7b and c. The simulation results are closer to the total pressure probe results than five-hole probe results, the data obtained from total pressure probe are the benchmark for CFD simulation. With the exception of measure technology reason, the main cause of total coefficients distribution cannot consistent well between simulation and experiment are the blade install angle and tip clearance uneven distribution, which described in Fig. 6, besides, the rotor–stator interface model in simulation is also the reason for the bad uniformity. The overall trend of the pressure coefficient distribution in spanwise is within a reasonable range.

In this section, numerical simulation grids strategy has been verified satisfy independence demanding, numerical simulation precision has also been analyzed and demonstrated the rationality for research the rotating instability. It is convincing that the experimental facility compressor blades geometry install angle deviation 1° is the reason for

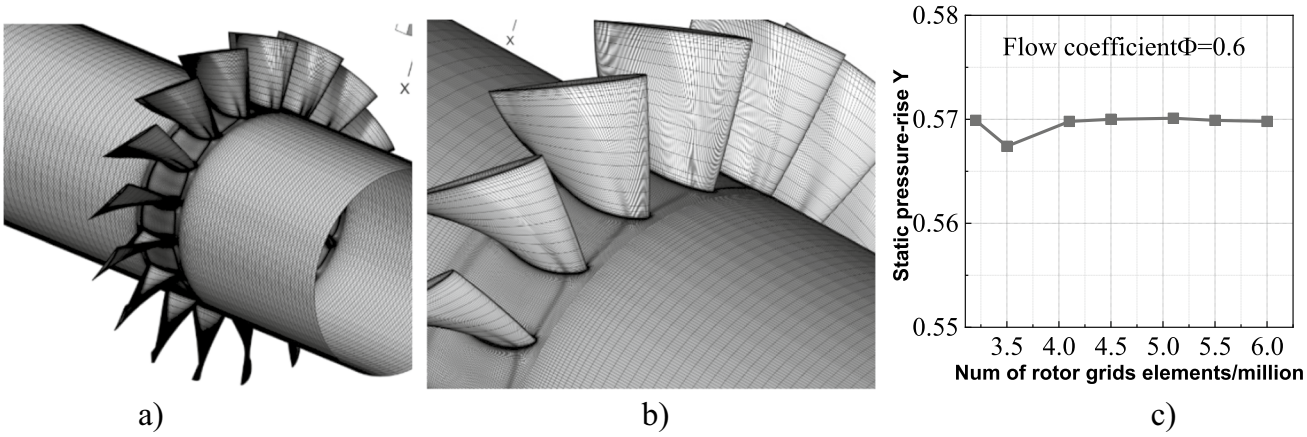

Fig. 5 Isolated-rotor calculation mesh **a** whole view of the mesh grid model **b** rotor view grid model **c** grids independence verify results

Table 2 Different levels used for grids independence study

Case No.	1	2	3	4	5	6	7
Number of grids/million	3.2	3.5	4.1	4.5	5.1	5.5	6

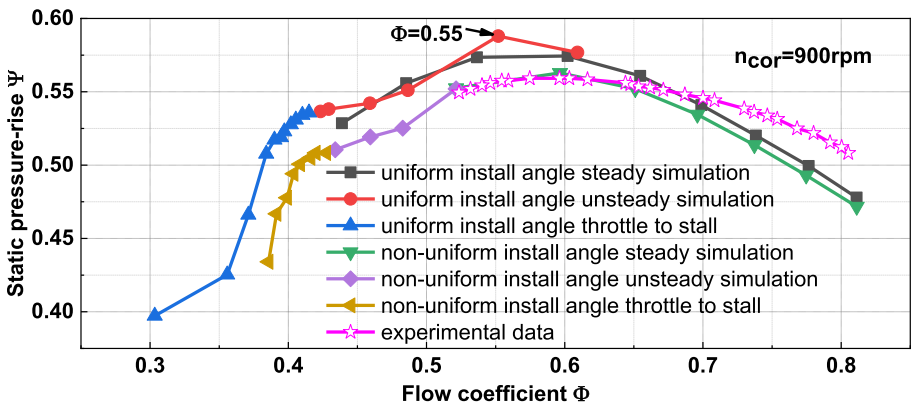

Fig. 6 Isolated-rotor simulation and experimental characteristic curve

the compressor fall into stall ahead to 0.55 flow coefficient. The numerical simulation model with uniform install angle blade predict the stall at 0.42 flow coefficient.

4 Results and discussions

4.1 Experimental results of rotating instability characteristic in the isolated rotor

The isolated-rotor compressor experiment is designed to reveal the leakage vortex propagation phenomenon in the blade passage and obtain the non-synchronous frequency band characteristic. Casing wall pressure sensors array and dynamic total pressure probe and SPIV have been utilized to study the rotating instability of leakage vortex spatial distribution. The overall characteristic of static pressure oscillation has been captured by the casing wall pressure root-mean-square (RMS) contour, which is shown in Fig. 8.

In Fig. 8a, at design point, the leakage vortex is propagated far from the adjacent downstream blade in the blade passage. The maximum region of pressure oscillation amplitude occurred from the leading edge to 30%chord length position are pointed as A shown in Fig. 8a. The B region which pointed out in Fig. 8a with black dotted line is an expanded leakage vortex. This expanding phenomenon means the leakage vortex is broken near the 80% chord length region. The leakage vortex trajectory which pointed out in Fig. 8b with red dotted line is almost parallel with the rotor frontal line indicate that the broken leakage vortex impacted on the adjacent downstream blade leading edge. The pressure oscillation amplitude at near stall point is higher than design point because leakage vortex has propagated and impact on the downstream blade leading edge. The broken leakage vortex caused pressure oscillation on the downstream blade pressure surface, much severer than the suction surface. The propagation trace of the leakage flow point to the trailing edge is shown in Fig. 8b A region, which is a typical represent of the spatial distribution characteristic of the tip leakage flow at near stall condition.

The B region, showed in Fig. 8b is caused by the suction surface corner separation vortex move in the radial direction to the tip region flow. This conclusion could be confirmed with Fig. 9.

The tip leakage vortex (TLV) and corner vortex radial direction motion are captured by the total pressure dynamic probe at the rotor outlet in Fig. 9. It is corresponding well to the casing wall pressure results. Besides, the pressure fluctuation distribution in the rotor outlet section surface is ensemble averaged through the lock-phase signal, assisted with radial motion total pressure probe. At near stall condition, where TLV is stronger and has a wider influence region till 0.75span radial position than that at design condition with a region till 0.9span. In Fig. 9, the spatial scale of the TLV steady distribution in radial and circulation direction are shown with pressure RMS value, obtained obviously distinguish of the TLV spatial distribution at design point and near stall point.

The SPIV measurement technology is utilized in this isolated-rotor compressor to get the tip region flow spatial distribution in axial and circulation direction. Besides, another aim of utilizing SPIV is to capture the leakage vortex propagation and broken characteristic in the blade passage. The normalized vorticity and streamwise velocity coefficient slice contours are shown in Figs. 10 and 11, respectively. The "streamwise" here is the same direction as the normal direction of the measurement slices. The streamwise velocity coefficient is the measured velocity that perpendicular to the slice and normalized by the tip velocity.

Vortex identification is based on λ_2 criterion in cylindrical coordinate system, which defined by the Eq. (1). The physical reasoning for this criterion is that, pressure tends to

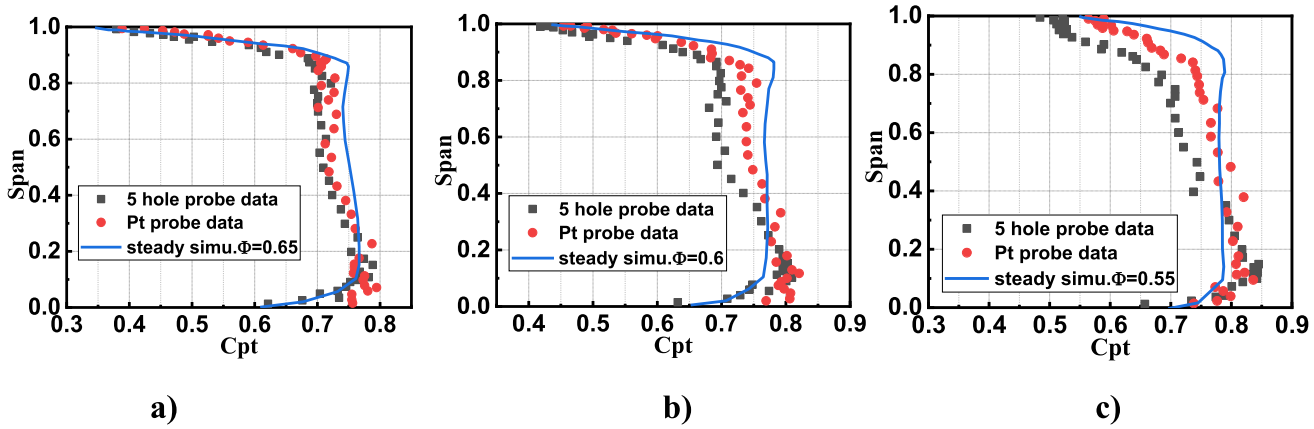

Fig. 7 Isolated-rotor outlet total pressure coefficients distribution in radial direction **a** $\Phi=0.65$; **b** $\Phi=0.60$; **c** $\Phi=0.55$

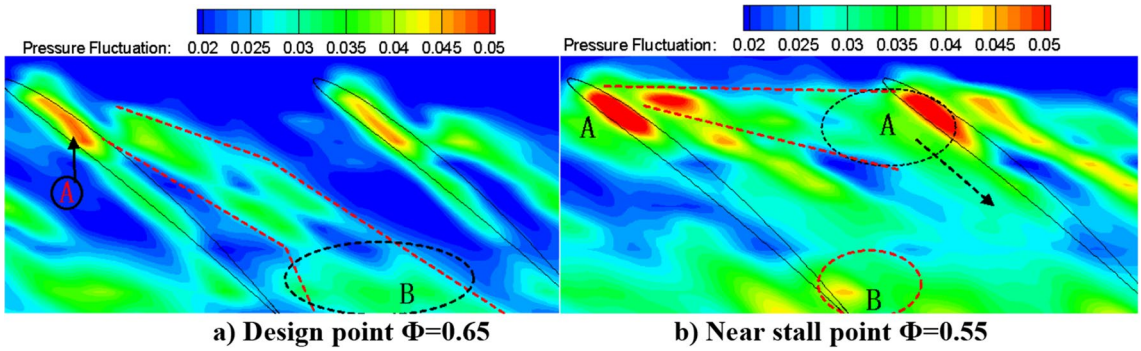

Fig. 8 Isolated-rotor tip region pressure oscillation

have a local minimum when the centrifugal force is balanced by the pressure force, consider only $S^2 + \Omega^2$ to determine the existence of a local pressure minimum due to vortical motion and define a vortex core as a connected region with two negative eigenvalues of $S^2 + \Omega^2$. S is the symmetric straining acceleration tensor of velocity gradient tensor ∇u, Ω is the asymmetric rotation acceleration tensor of ∇u. Since $S^2 + \Omega^2$ is symmetric, it has real eigenvalues only. If $\lambda_1, \lambda_2, \lambda_3$ are the eigenvalues and $\lambda_1 \geq \lambda_2 \geq \lambda_3$, the $\lambda_2 < 0$ should be the requirement that within the vortex core. In this paper, the two dimension λ_2 solution is based on the Liu [40] promoted method, showed in Eq. (1), where $\frac{\partial V_r}{\partial r}$ is the radial velocity gradient, $\frac{\partial V_\theta}{r\partial\theta}$ is the tangential velocity gradient, $\frac{\partial V_r}{\partial\theta}$ is radial velocity gradient in tangential direction, $\frac{\partial V_\theta}{\partial r}$ is the tangential velocity gradient in radial direction.

$$\lambda_2 = \left(\frac{\partial V_r}{\partial r}\right)^2 + \left(\frac{\partial V_\theta}{r\partial\theta}\right)^2 + 2 \cdot \frac{\partial V_r}{r\partial\theta}\frac{\partial V_\theta}{\partial r} \tag{1}$$

The SPIV results in the blade passage showed a clear leakage vortex at two operating conditions. In Fig. 10a, the vorticity contour showed the leakage vortex has no impact on the adjacent downstream blade in the passage and the streamwise velocity in the tip region is low. This phenomenon is corresponding to the casing wall pressure contour in Fig. 8a. In Fig. 10b, the leakage vortex started broken at the leading edge 50% chord length position and invaded to the pressure surface of the near blade. The streamwise velocity in Fig. 11b showed the velocity in the leakage vortex core is about 0.5. The low streamwise velocity region at near stall condition, obviously becoming larger than the design point condition. It means a larger scope of blocking has formed at near stall point.

The SPIV results illustrate that the leakage vortex shedding position at near stall is closer to the leading edge. Compared with the casing wall pressure which showed in Fig. 8, there are no obviously corresponding TLV impingement near the leading edge of the adjacent blade in Figs. 10 and 11. This is due to the occlusion structure which designed to eliminate the SPIV window reflect light. This operation caused the SPIV section could not fully extended to casing wall. The impaction on the near blade pressure surface also has been captured by the SPIV technology. The design point results explained that the weak leakage flow has no impact on the near blade pressure surface. The SPIV system is limited by the low frequency laser and cameras. The

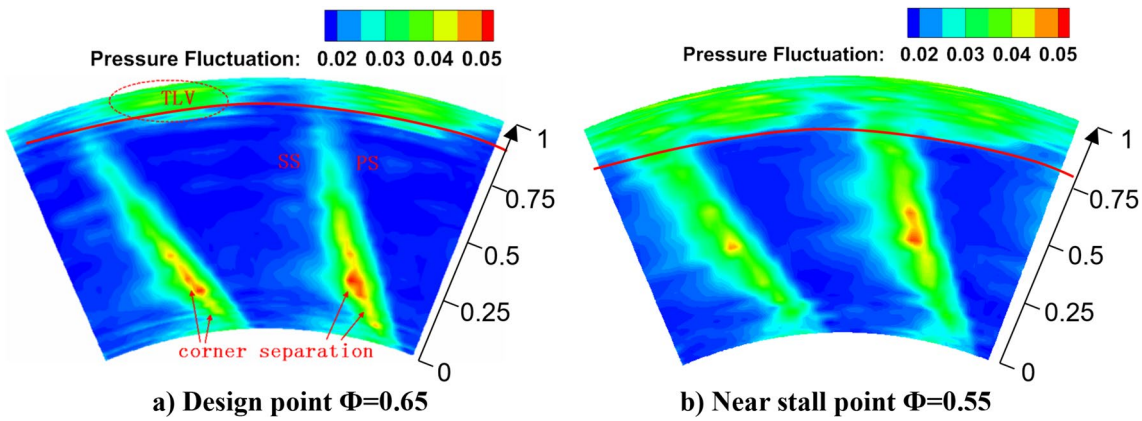

Fig. 9 Isolated-rotor outlet total pressure oscillation

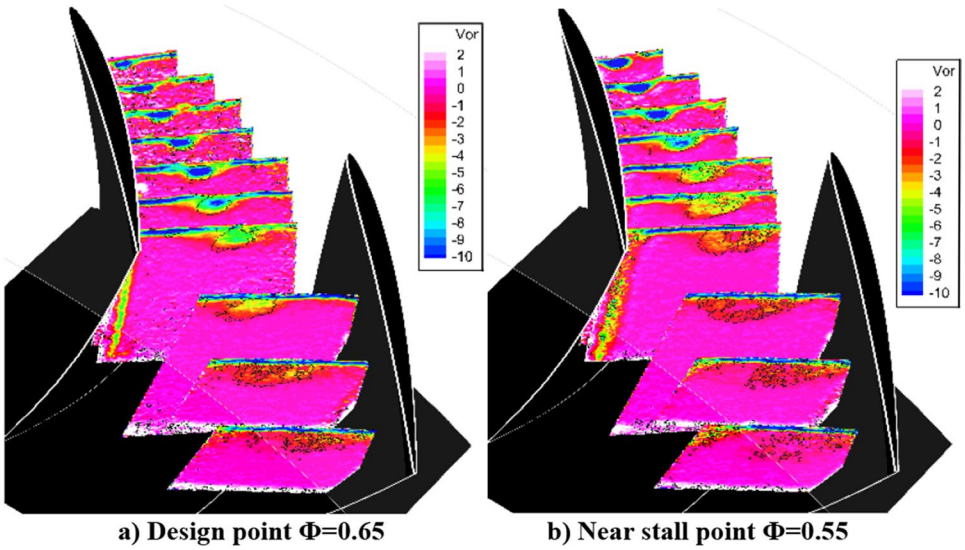

Fig. 10 Distribution of normalized vorticity (Black solid line indicates the threshold where $\lambda_2 = -30$)

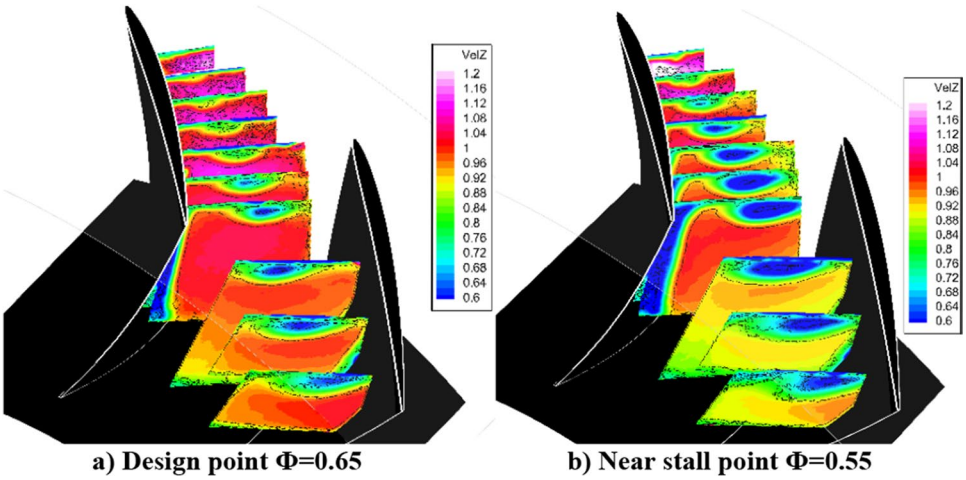

Fig. 11 Streamwise velocity coefficient in rotor passage

SPIV flow are all averaged steady results and impossible to get the shedding frequency of the tip leakage vortex. But the steady flow field still improved valuable information of leakage vortex.

The casing wall pressure, dynamic pressure probe results and SPIV results represent the vortex propagation characteristic. The instability is not occurred only in a single passage. It is a vortex circulation propagation phenomenon. To clarify and further research the phenomenon caused pressure oscillation, a frequency spectrum is executed with dynamic total pressure probe data. The frequency spectrum analysis can help to distinguish and obtain all the pressure oscillation components. This procedure can improve the understanding of the tip leakage flow unsteadiness characteristics.

To analyze the frequency region characteristic of the passage flow, Fast Fourier Transform (FFT) is utilized as an important tool. In Fig. 12, the raw pressure signal and frequency spectrums of the dynamic total pressure probe from the rotor outlet flow are shown. In the picture, there are some abbreviated variables such as f_{rot}, BPF, where the f_{rot} means the rotor rotation frequency which defined number of rotor-turns in one second, BPF is represent the blade pass frequency.

In Fig. 12, the blade pass frequency (BPF) is remarkable. A frequency band with centered 0.4BPF about 75–150 Hz which pointed out with RI has a high amplitude. This phenomenon is similar to Mailach [24], Marz [25] and Biela [26] reported rotating instability frequency spectrum characteristics. Rotating instability is corresponding to the raw data at 96% span with blue arrows pointed out large scale disturbance. At the 60% span, the frequency spectrum is flat at the RI frequency region. It indicated that the RI disturbance is not existence at 60% span.

The waterfall plotted all the span measured pressure signal frequency spectrums are shown in Fig. 13.

The rotating instability occurred at design point and near stall point. Compared with design point, the near stall point has a lager amplitude and more wide frequency band. The

scope of tip region which influenced by RI is 10% span at design point but 20% span at near stall point. In the radial direction, RI frequency band has also occurred in blade root region and 50% span region, where pointed out in Fig. 13 B region. This phenomenon is corresponding to the corner separation flow. The corner separation flow moved in the radial direction is more seriously when the flow velocity decreased. The tip leakage vortex broken and blade root corner unsteady separation flow are all showed rotating instability characteristic.

There are two typical vortex broken forms, stable bubble broken and spiral vortex broken. The spiral vortex broken form will create large scale turbulence trace and wide frequency spectrum characteristic [41]. The tip region rotating instability is caused by the leakage vortex spiral broken and the corner vortex in this article.

4.2 Numerical simulation of tip leakage flow and circumference propagated instability characteristic

The experimental results in 4.1 showed an unsteady broken of the tip leakage vortex. To further research the tip leakage flow, an isolated-rotor annular simulation has been obtained with high performance computer. This section focused on the mechanism of rotating instability and the propagation process in the circulation direction. The numerical simulation of rotating instability is based on the isolated rotor near stall condition, which $\mathbf{\Phi = 0.55}$.

To create the relationship between casing wall pressure and the tip leakage vortex, the absolute coordinate data has been shifted to relative coordinate system. Casing wall pressure frequency spectrum in fixed coordinate system contains several frequency components are shown in Fig. 14a. In Fig. 14a, the 255 Hz is the blade pass frequency. The pressure frequency spectrum contains 213.1 Hz(0.84BPF) in Fig. 14b. This pressure extracted position is located at the blade leading edge position in a rotate coordinate system. This experiment data of casing wall pressure are utilized to compare with simulation casing wall pressure.

The frequency analysis of the numerical simulation is based on the pressure frequency spectrum showed in Fig. 14b. In Fig. 15, the coefficient of static pressure at 98% span section where a distance from the blade tip 1 mm and from the casing wall 4 mm are shown. A high static pressure spot marked as B1 occurred at the leading edge of the blade passage are shown in Fig. 15b–d. The static pressure spot move to the pressure surface in a passage cycle. The static pressure spot affected region expanding and the static pressure rise becoming larger at the spot moving process. The spot hit on the downstream nearly blades are shown in Fig. 15 such as B region a, B1 region e.

A low static pressure spot is closed to the high static pressure spot on the pressure surface. The low static pressure spot is pointed as A region in Fig. 15. The cycle of single passage is calculated by Eq. (2). The static pressure spots have a cyclical process which followed a frequency 213 Hz (0.84BPF) which calculated by Eq. (3).

$$T = \frac{1}{\left(\left(\frac{n}{60}\right) \times N\right)} \tag{2}$$

$$f = \frac{n}{60} \times N \times t1 \tag{3}$$

T is the cycle of isolated-rotor blade passage. N is the blade number of the isolated-rotor. The rotating speed is n with unit (RPM). The t1 is equal to 1.2 T which found in

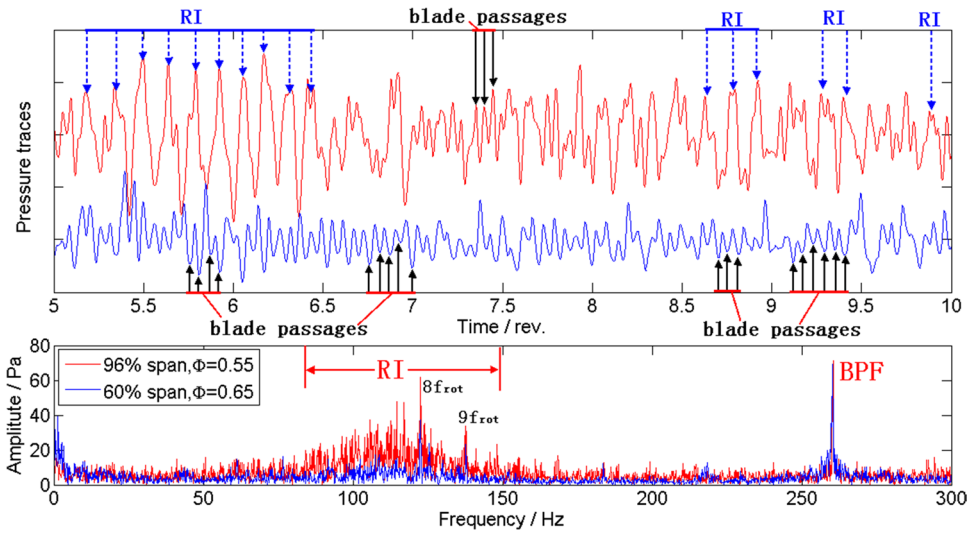

Fig. 12 Isolated-rotor outlet dynamic total pressure probe raw data and frequency spectrums at 96% and 60% span

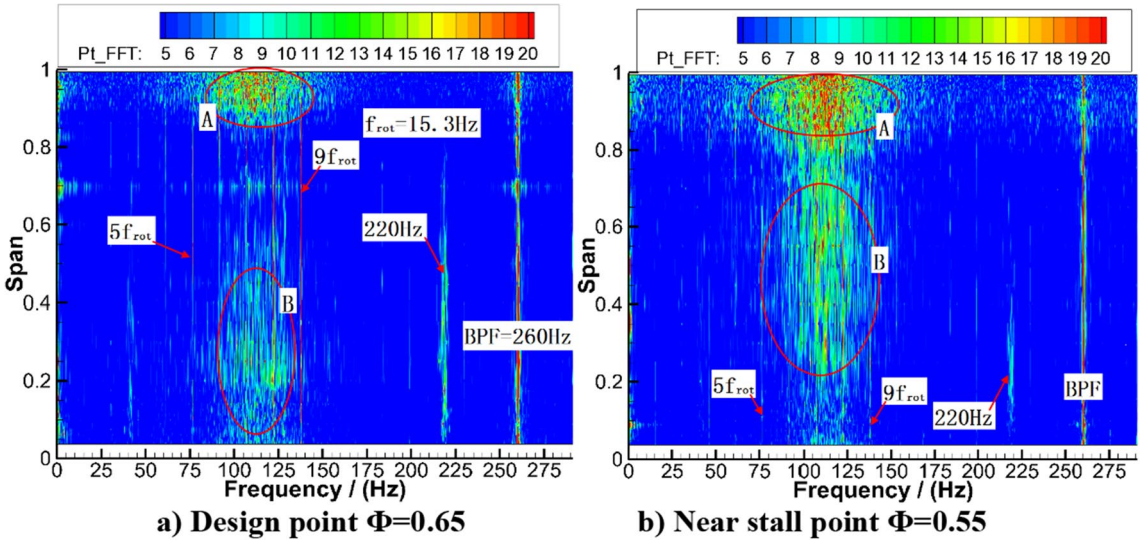

Fig. 13 Isolated-rotor outlet pressure frequency spectrum at radial direction various position

Fig. 15. In this simulation, the n is equal to 900 RPM, the *N* is equal to 17.

The velocity vectors in tangent direction in the blade passage that same as Fig. 16 are shown in Fig. 17. A low-speed vortex region occurred at the middle and leading edge of the passage. The low-speed region has moved and hit on the pressure surface. This trace of low-speed region is the same as the static pressure spot.

In Fig. 17, showed entropy rise contours, it is the corresponding blade passage with Figs. 15 and 16. The entropy rise contours are shown in a blade passage cycle. The high entropy rise regions are pointed out with a black arrow from 0 to 1 T. The entropy rise region could be set as a leakage vortex. A reference line on the suction surface is created to get the angle between leakage vortex and the reference line are shown in Fig. 17. The angle changed in a cycle is corresponding to the leakage vortex swing in the passage. The angle between leakage vortex and frontal line becoming smaller from 0 to 0.4 T explained that the leakage vortex has been enhanced. This phenomenon is related with the increased pressure surface leading edge static pressure showed in Fig. 15. The intersection angle between frontal line and leakage vortex line becoming larger from 0.8 to 1 T explained that the leakage vortex weakened. This phenomenon is related with the static pressure spot move to the blade trailing edge, which showed in Fig. 15c and d. The leakage vortex and the nearby blade pressure surface static pressure spot position have an interaction that caused the angle between the vortex line and the frontal line cyclical oscillation.

The cyclical changed static pressure spot position caused the tip region pressure difference between the suction surface and the pressure surface cyclical oscillation. Leakage velocity is a component of tip leakage flow velocity perpendicular to chord direction. The coefficients of pressure

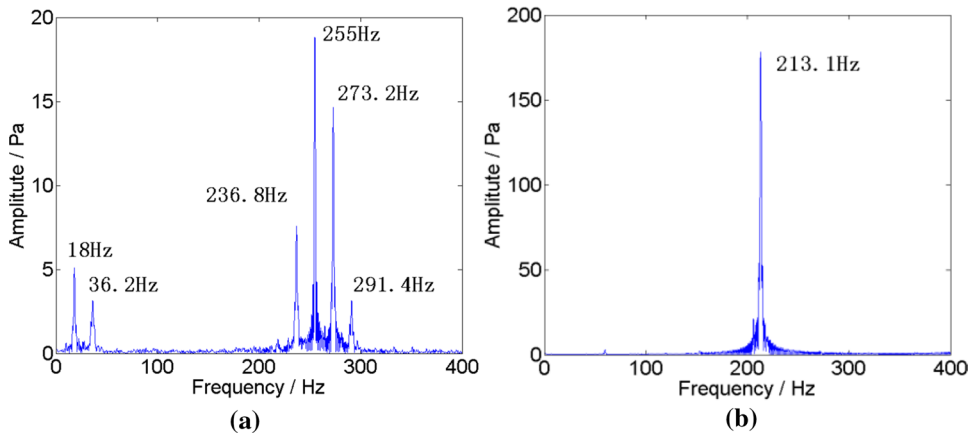

Fig. 14 Isolated-rotor outlet casing wall pressure frequency spectrum, experimental results **a** Frequency spectrum in fixed coordinate system **b** Frequency spectrum in rotate coordinate system

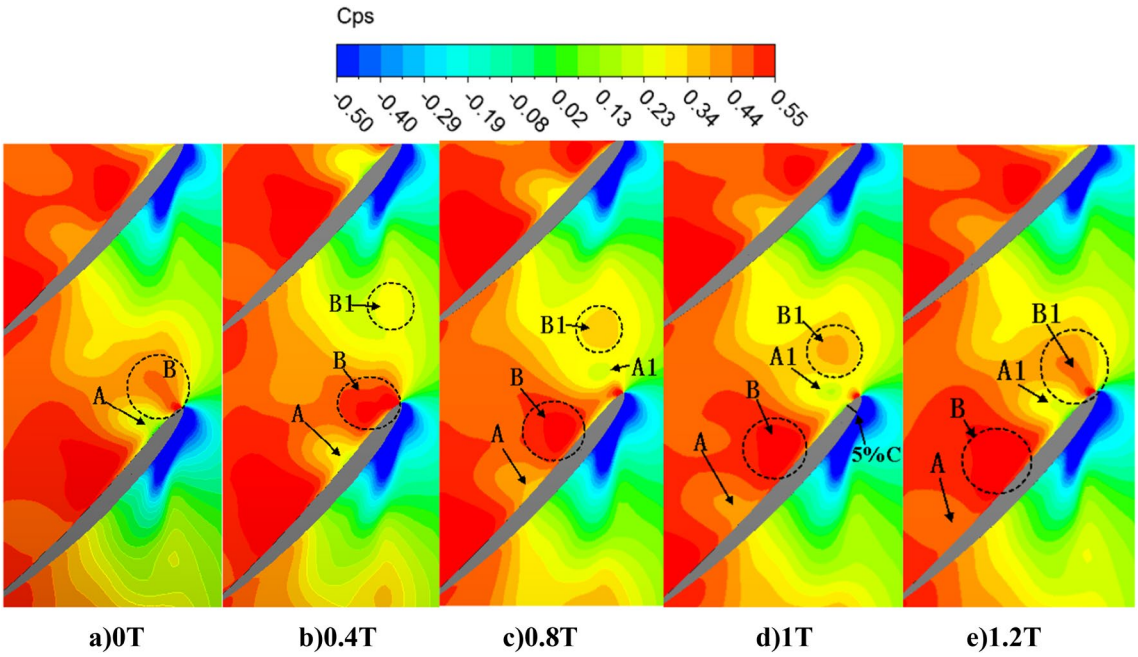

Fig. 15 98% span blade passage static pressure variation with time, T is one cycle of blade rotate through a passage

and the tip leakage velocity oscillation curves are shown in Fig. 18.

Between the peak value of the leakage velocity and the peak value of the static pressure coefficients has a time difference. It means that the leakage occurred lagging behind the pressure difference. The pressure difference's cyclical oscillation caused the leakage vortex swing.

Mailach [24] holds that the cyclical oscillation of the leakage vortex hit on the downstream blade pressure surface caused a phase difference between the nearby blade passages. This flow chain phenomenon is the formation mechanism of rotating instability.

In Fig. 19, two contours of static pressure coefficient and entropy rise in five blade passages at 0 T are shown.

The vortex propagation characteristics in circulation direction are different in blade passages at the same time. The static pressure coefficients phase difference distribution in the blade 2 and blade 3, blade 6 and blade 7, blade 7 and blade 8 passages are small. It means that there is a 4–5 passages length circulation pressure wave. The wave number is about 3–5.

To clarify the pressure wave propagation characteristic in the rotor, the space Fast Fourier Transform (FFT) method is utilized to get the wave number. The results are

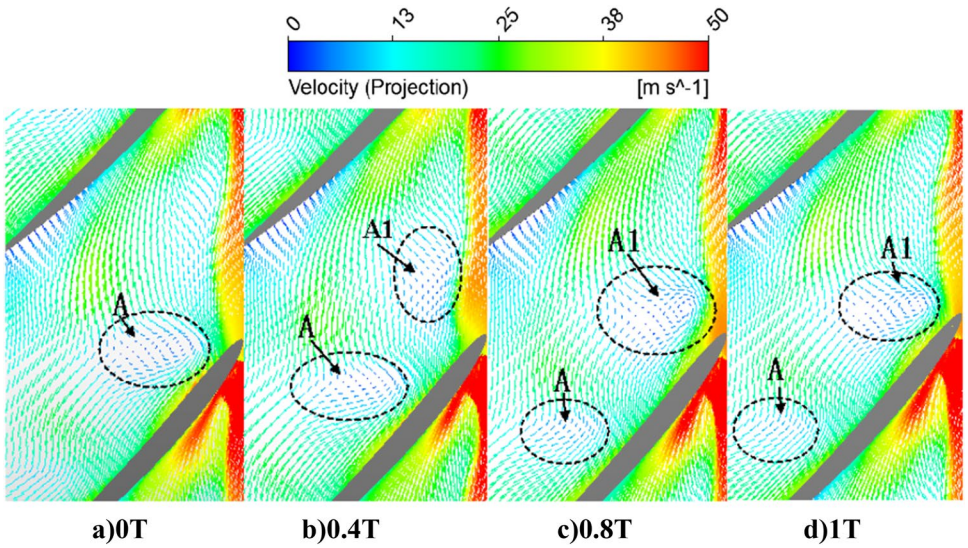

Fig. 16 98% span blade passage velocity vector variation with time, T is one cycle of blade rotate through a passage

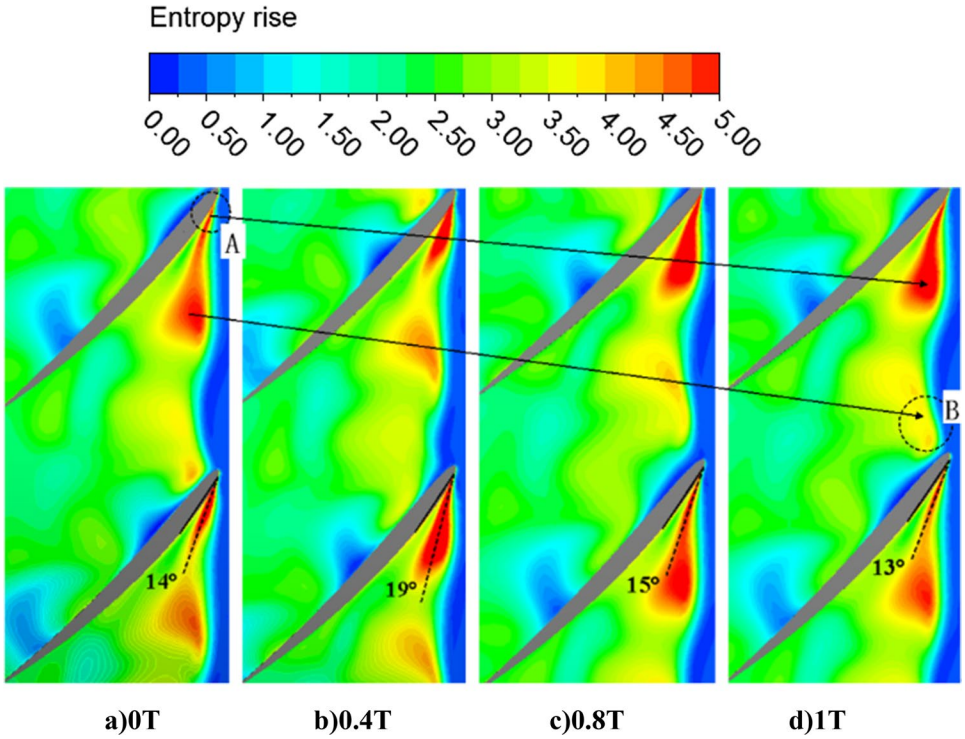

Fig. 17 98% span blade passage entropy rise variation with time, T is one cycle of blade rotate through a passage

shown in Fig. 20. The blade number is 17. The wave number 17 is clearly shown in Fig. 20. Wave number 4 is also distinguished in Fig. 20. Wave numbers 13, 30, 34 are all the superposition mode of 17 and 4. It can be concluded that there are 4 disturbance waves in the rotor circulation passages.

The pressure distribution in circulation direction at 10% chord length casing wall is shown in Fig. 21. The data have been executed space filter with end wave number 4 and space Fast Fourier Transform (FFT). The wave shape with four peaks are distinguish from 0° to 360° in circulation direction. The pressure wave 4 is corresponding to the pressure difference wave with the same frequency 213.1 Hz (0.84BPF) showed in Fig. 14b in relative coordinate system.

The rotating instability characteristic has been clarified from upon simulation and experiment research. The vortex in the blade passage experienced a process that from produce to propagation and broken. The mechanisms of the flow are revealed in the following analysis. The flow structures in near blade passage are shown in Fig. 22. Three blade passages are selected to illustrate the vortex developmental process.

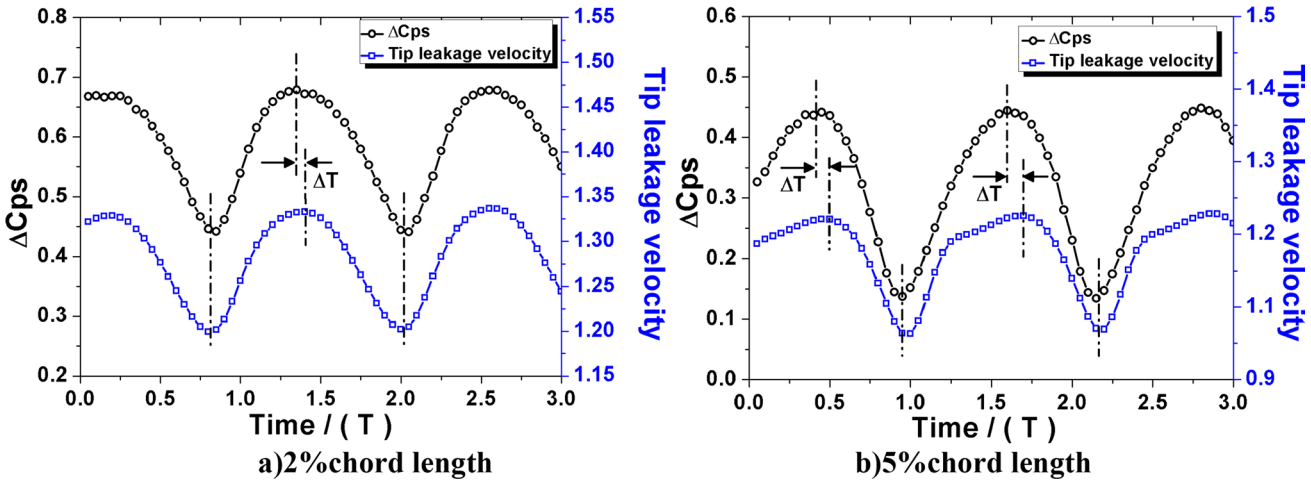

Fig. 18 98% span blade passage velocity vector variation with time, T is one cycle of blade rotate through a passage

There is a focused vorticity caused by leakage vortex rolling and concentrating at chord length from 10 to 40% in Fig. 22 pointed out as A, B, C passages which is similar to the process showed in Fig. 19. The focused vorticity disappeared from 50% chord length till 60% chord length where the streamline becoming straight.

In Fig. 22a, the A region represent the leakage vortex broken down and move to the pressure surface absorbed by the low-speed leakage flow. The broken vortex has mixed with the main flow in the passage and disappeared at the trailing edge. At the trailing edge, leakage vortex is rather weak to supplement flow to sustain the A region vortex expanding. The leakage vortex shedding from the leading edge then propagate to the pressure surface and disappeared, this process is shown in Fig. 22.

At the near stall point, the unsteadies of the leakage vortex is much more complex. The leakage vortex development in the passage is revealed in Fig. 23 at near stall point.

In Fig. 23, the leakage vortex shedding and broken are more obviously at near stall point. There are three vortex A, B, C existence in the passage at the same time. The vortex labeled A expanded rapidly when the vortex B move to downstream, meanwhile the vortex C mixed and dissipation are shown in Fig. 23b.

The vortex broken position at near stall point which pointed out in Fig. 23 A region is at 40%-50%chord length. The vortex broken position is closer to the upstream of leakage vortex core, compared with the design point in Fig. 22 A region at 60% chord length.

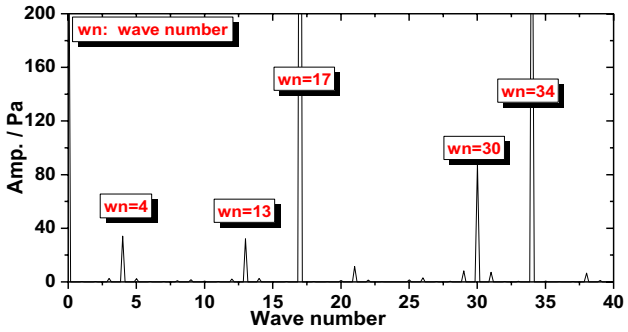

Fig. 20 10% chord length circulation pressure signal space FFT

4.3 Discussions

The rotating instability characteristic and mechanism has been illustrated and discussed with experiment and simulation method. Meaningful results have been obtained and showed in upon paragraphs.

Casing wall pressure RMS value and SPIV captured ensemble averaged vorticity result have illustrated the tip leakage vortex spatial distribution characteristic at different flow rates. With the help of casing wall pressure sensor and total pressure probe, dynamic pressure oscillation non-synchronous frequency is captured in the tip region. Besides, the ensemble probe data acquired in spanwise very intuitively showed the radial spatial distribution region at design and near stall condition, respectively. But, limited by the experimental techniques, detailed analysis is hard to pursue, such as dynamic analysis of the SPIV result, vortex swing circle analysis.

Fig. 19 98% span blade passage velocity vector variation with time, T is one cycle of blade rotate through a passage

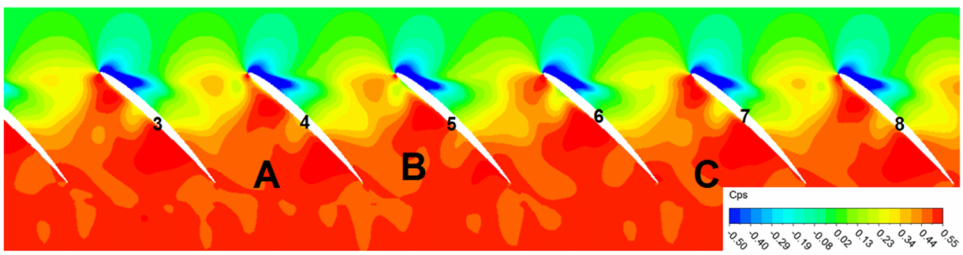

a) Static pressure coefficient

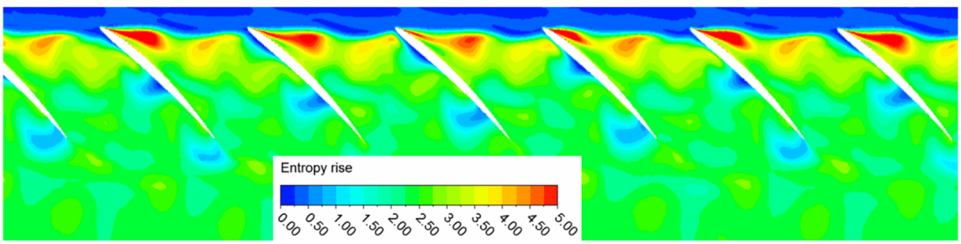

b) Entropy increase

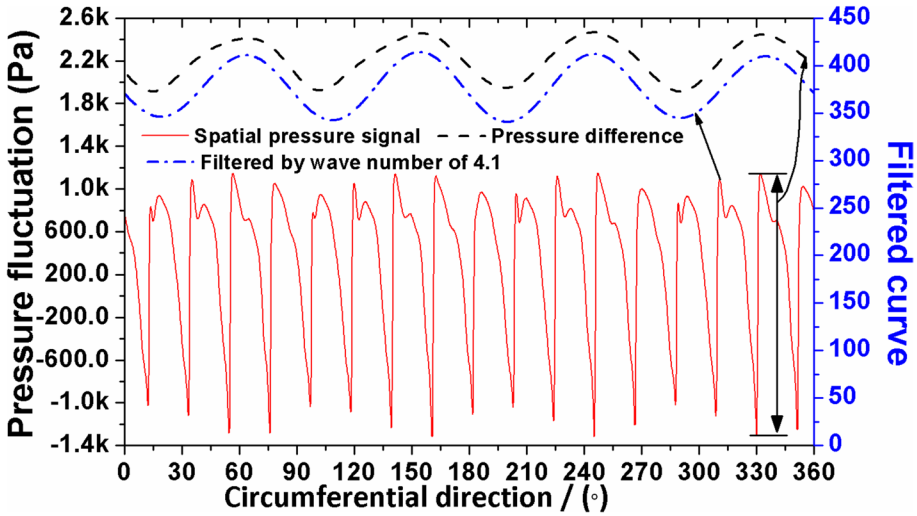

Fig. 21 pressure oscillation (origin pressure subtraction average data) in circulation direction at 10% chord length casing wall

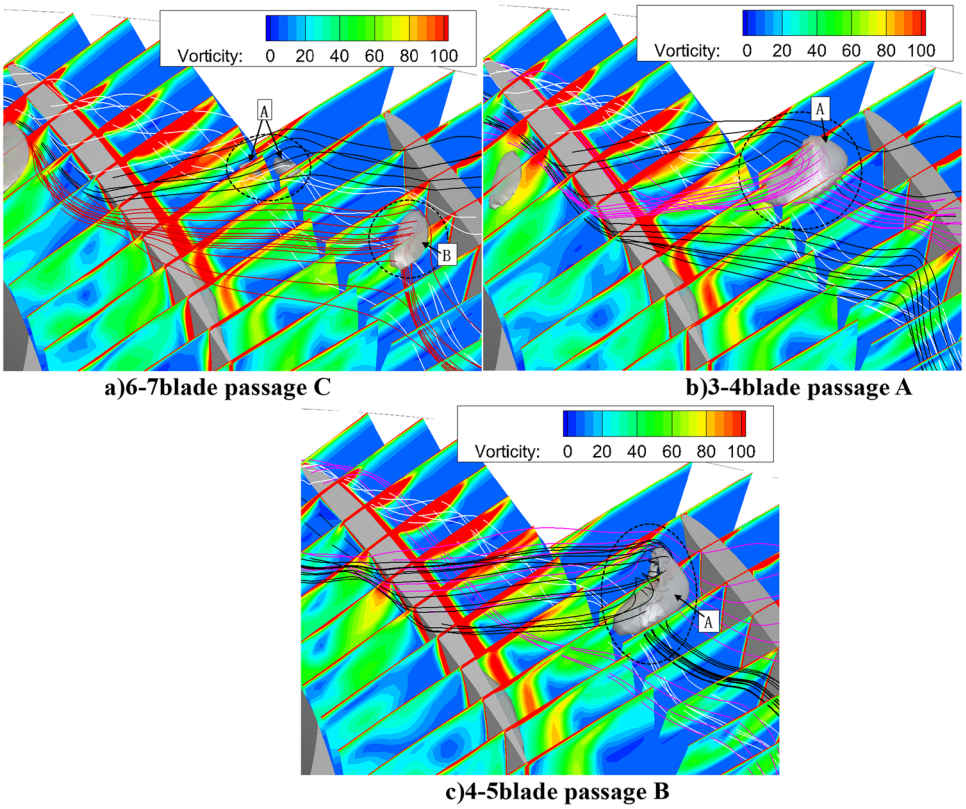

Fig. 22 Dimensionless vorticity and dimensionless velocity $V/U_{tip} = 0.1$ iso-surface and streamline

Numerical simulation has a good performance for capturing the spatial and temporal resolution of the tip leakage vortex, spatial distribution characteristic and temporal frequency analysis of casing pressure has a good consistence with experiment result. Detailed vortex line and blade frontal line intersection angle analysis is feasible from the numerical simulation, gives better understanding of the leakage vortex swing in spatial and temporal dimensions, which is a very important criterion for design and near stall condition.

Detailed analysis of the leakage vortex propagation frequency and wave number are executed, the objective of clarify the leakage vortex propagation and broken caused non-synchronous characteristic is achieved. Experimental techniques and numerical simulation are mutual auxiliary to get the tip leakage vortex spatial distribution in radial and circular direction, get the time frequency evolution characteristic of tip leakage flow in the passage. Clear contour image and time region pressure data that captured by casing wall sensor and probe provided convince results that

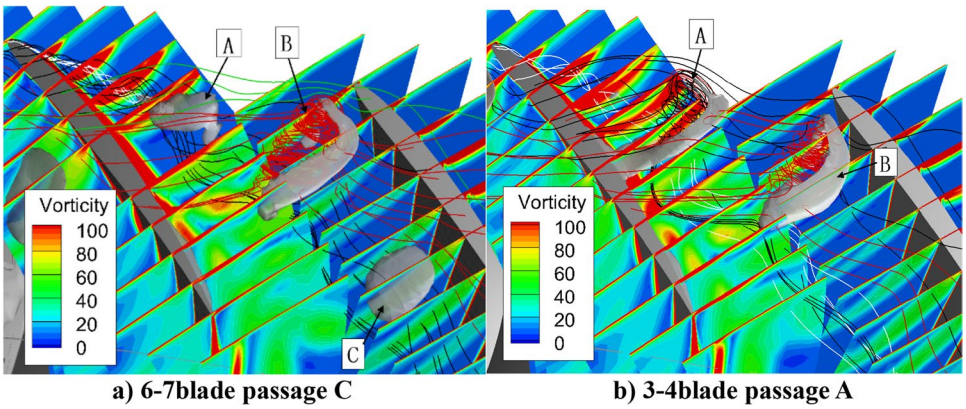

a) 6-7blade passage C b) 3-4blade passage A

Fig. 23 Near stall, vorticity and streamline and dimensionless velocity $V/U_{tip}=0.1$ iso-surface

demonstrated the tip leakage flow characteristic at near stall condition where occurred rotating instability.

In this paper, comprehensive and appropriate experiment techniques and validated numerical simulation methods could help to reach the objectives about the rotating instability of tip leakage vortex in spatial and temporal dimensions.

5 Conclusions

The present work applies casing wall pressure sensors, total pressure probe, five-hole probe, SPIV, numerical simulation, and their variants to the unsteady tip leakage flow analysis of a low-speed axial compressor. First, the differences in design and near stall point identified spatial and temporal structures are compared comprehensively. On this basis, the tip leakage flow and propagating circulation are also revealed by means of these techniques. The obtained conclusions are summarized as follows:

1) Casing wall pressure data and ensemble-averaged SPIV results demonstrated that the leakage vortex at near stall has a greater influence scope than the design point in the blade passage. The leakage vortex broken position is advanced at near stall compared with the design point. Fast Fourier Transform has been executed for the casing wall presser sensor data, 213.1 Hz (0.84BPF) frequency components is obviously at near stall condition.
2) The dynamic total pressure probe frequency spectrum results showed a conclusion that rotating instability occurred in the tip region. The tip leakage vortex (TLV) and corner vortex radial direction distribution are captured by the total pressure dynamic probe at the rotor outlet. At near stall condition, the TLV influenced region should expanded to 80% span from the casing wall. At design point, the TLV influenced region distribution in upon 92% span. It indicated that the RI disturbance is not existence at 60% span. The non-synchronous characteristics 0.4BPF frequency band of the tip flow are found by the dynamic total pressure probe.
3) Considering the circulation propagation of the leakage vortex instability and the leakage vortex dynamic motion characteristic, a numerical simulation with commercial codes is essential for further the comprehensive of non-synchronous disturbance. A detailed analysis of the leakage vortex propagation in streamwise and circulation direction showed that the rotating instability occurred at near stall point, with a circulation propagation phenomenon. The frequency of the vortex oscillation in the passage has been captured, 213 Hz (0.84BPF), it is corresponding to the casing wall non-synchronous pressure characteristic.
4) The leakage vortex has an important influence on the pressure difference between the pressure surface and suction surface, which is an important reason for the rotating instability. Circumferentially propagating leakage vortex influenced on near blade caused a pressure fluctuation phase difference between nearby blades. Leakage vortex broken position becoming advanced and the angle between frontal line and vortex propagation direction decreased are the main reason for rotating instability.
5) The leakage vortex temporal and spatial swing phenomenon have been captured by the numerical simulation, the intersection angle between vortex line and blade frontal line has variety from 13° to 19° in a period. There is a focused vorticity caused by leakage vortex rolling and concentrating at chord length from 10 to 40%. The focused vorticity disappeared from 50% chord length till 60% chord length where the streamline becoming straight.

Simulation results helped to capture the leakage vortex propagation process in blade passages. Experimental and simulation methods are interrelated and mutual confirmed to explain the tip leakage flow and rotating instability. Reached the objective of clarify the generation mechanism

of non-synchronous tip flow characteristic and rotating instability disturbance propagation in the rotor. In a word, the circular propagation vortex at near stall point caused a pressure oscillation on the adjacent downstream rotor blade surface. This leakage vortex broken position ahead to the leading edge of the adjacent downstream blade is the main caution for rotating instability.

5.1 Future works

Although this research about the tip leakage vortex caused flow instability characteristic has adopted much means such as probe, SPIV, casing wall pressure sensors, more resolution ratio and detailed flow field measurements such as high frequency SPIV, and LES or DES turbulence model should be leaded into this research in the future research. Based on the high-resolution data from experimental technology, the tip leakage flow structures which induced the rotating instability and non-synchronous vibration should be extracted through data driven decomposition methods which able to analyze the main flow structure with its frequency information, corresponding to the non-synchronous instability frequency.

Acknowledgements The authors gratefully acknowledge the support of National Major Science and Technology Projects of China (2017-V-0016-0068), National Major Science and Technology Projects of China (2017-II-0009-0023), National Natural Science Foundation of China (No. 51776011).

References

1. Moller D, Schiffer HP (2020) On the mechanism of spike stall inception and near stall non-synchronous vibration in an axial compressor. In: Proceedings of ASME Turbo Expo 2020, GT2020–14711
2. Brandstetter C, Stapelfeldt S (2021) Analysis of a linear model for non-synchronous vibrations near stall. Int J Turbomach Propul Power 6(3):26. https://doi.org/10.3390/ijtpp6030026
3. Jiaye Gan, Im HS (2014) Investigation of a compressor rotor non-synchronous vibration with and without fluid structure interaction, In: Proceedings of ASME Turbo Expo 2014: turbine technical conference and exposition, Dusseldorf, 26478
4. Thomassin J, Vo Huu Duc (2014) Blade tip clearance flow and compressor NSV: The jet core feedback theory as the coupling mechanism. In: Proceedings of GT2007 ASME Turbo Expo 2007: power for land, sea and air, montreal, pp 27286
5. Huu Duc V (2010) Role of tip clearance flow in rotating instabilities and nonsynchronous vibration. J Propul Power 26:556–561. https://doi.org/10.2514/1.26709
6. Holzinger F, Wartzek F (2016) Self-excited blade vibration experimentally investigated in transonic compressors: rotating instabilities and flutter. In: Proceedings of ASME Turbo Expo 2015: turbine technical conference and exposition, Montreal, 43628
7. Fiquet AL, Aubert S, Brandstetter C et al (2021) Acoustic resonance in an axial multistage compressor leading to non-synchronous blade vibration. J Turbomach 143:191014
8. Zhou Di, Wang X, Chen J et al (2015) Sound generation by non-synchronously oscillating rotor blades in turbomachinery. J Sound Vib 355:150–171. https://doi.org/10.1016/j.jsv.2015.06.018
9. Baumgartner M, Kameier F, Hourmouziadis J (1995) Non-engine order blade vibration in a high pressure compressor. In: 12th International symposium on airbreathing engine
10. Kielb RE, Barter JW, Thomas JP (2003) Blade excitation by aerodynamic instabilities- a compressor blade study. Proceed ASME 4:399–406. https://doi.org/10.1115/GT2003-38634
11. Brandstetter C, Jungst CM, Schiffer HP (2017) Measurement of radial vortices, spill forward and vortex breakdown in a transonic compressor, In: Proceedings of ASME, Vol 7B, GT2017–64576
12. Han L, Wei D, Wang Y (2020) Locked-in phenomenon between tip clearance flow instabilities and enforced blade motion in axial transonic compressor rotors, In: Proceedings of ASME, Vol 10A, GT2020–16050.
13. Stapelfeldt S, Brandstetter C (2020) Non-synchronous vibration in axial compressors: lock-in mechanism and semi-analytical model. J Sound Vibrat 488:115649. https://doi.org/10.1016/j.jsv.2020.115649
14. Han L, Wei D, Wang Y (2021) Lock-in phenomenon of tip clearance flow and its influence on aerodynamic damping under specified vibration on an axial transonic compressor rotor. Chinese J Aeronaut 2:185–200. https://doi.org/10.1016/j.cja.2021.02.016
15. Li H, Zheng Q, Chen Z et al (2021) The role of radial secondary flow in the process of rotating stall for a 15-stage axial compressor. Aerosp Sci Technol 115:106752. https://doi.org/10.1016/j.ast.2021.106752
16. He X, Fang Z, Rigas G et al (2021) "Spectral proper orthogonal decomposition of compressor tip leakage flow. Phys Fluid 33:102105. https://doi.org/10.1063/5.0065929
17. Zheng Y, Gao Q, Yang H (2023) Non-synchronous blade vibration analysis of a transonic fan. Chinese J Aeronaut 36(1):178–190. https://doi.org/10.1016/j.cja.2022.04.011
18. Clark ST, Kielb RE, Hall KC (2012) Developing a reduced-order model to understand non-synchronous vibration (NSV)in turbomachinery. In: Proceedings of ASME Paper, Vol 7, GT2012–68145, pp.1373–1382. https://doi.org/10.1115/GT2012-68145
19. Wang D (2016) Study on the dynamics of vibrations for the aero-engine compressor blades considered the fluid-structure interactions Ph.D. Harbin Institute of Technology, Harbin
20. Hoskoti L, Misra A, Sucheendran MM (2018) Frequency lock-in during vortex induced vibration of a rotating blade. J Fluid Struct 80:145–164. https://doi.org/10.1016/j.jfluidstructs.2018.03.011
21. Im HS, Zha G (2012) Effects of rotor tip clearance on tip clearance flow potentially leading to NSV in an axial compressor, In: Proceedings of ASME Paper, Vol 7, GT2012–68148, pp.1383–1394
22. Spiker MA, Kielb RE (2008) Efficient design method for non-synchronous vibrations using enforced motion, In: Proceedings of ASME paper, Vol 5, GT2008–50599, pp.735–747
23. Mailach R, Sauer H, Vogeler K (2001) The periodical interaction of the tip clearance flow in the blade rows of axial compressors, In: Proceedings of ASME Paper, Vol 1, 2001-GT-0299
24. Mailach R, Lehmann I, Vogeler K (2001) Rotating instabilities in an axial compressor originating from the fluctuating blade tip vortex. J Turbomach 123:453–463. https://doi.org/10.1115/1.1370160
25. Marz J, Chunill H, Wolfgang N (2002) An experimental and numerical investigation into the mechanisms of rotating instability. J Turbomach 124:367–375. https://doi.org/10.1115/1.1460915
26. Biela C, Muller MW, Schiffer HP (2008) Unsteady pressure measurement in a single stage axial transonic compressor near the stability limit. In: Proceedings of ASME, Vol 6, GT2008–50245, pp 157–165

27. Ma H, Jiang H (1997) 3D turbulent flow at compressor rotor exit under different flow conditions. J Aerosp Power 12:268–272
28. Yang Z, Wu Y, Ouyang H (2022) Investigation on mode characteristica of rotating instability and rotating stall in an axial compressor. J Turbomach 144:061010
29. Tu B, Zhang X, Hu J et al (2021) Analysis methods for aerodynamic instability detection on multistage axial compressor. Int J Aerosp Eng. https://doi.org/10.1155/2021/8893792
30. Ma H, Wei W, Ottavy X (2017) Experimental investigation of flow field in a laboratory-scale compressor. Chin J Aeronaut 30:31–46. https://doi.org/10.1016/j.cja.2016.09.016
31. Rodrigues M, Soulat L, Paoletti B, Ottavy X, Brandstetter C (2021) Aerodynamic investigation of a composite low-speed fan for UHBR application. J Turbomach. https://doi.org/10.1115/14050671
32. Ma H, Jiang H (2000) Unsteady static pressure field on the tip endwall of an axial-flow compressor rotor passage. J Eng Thermalphys 21:42–45
33. Liu JM, Holste F, Neise W (1996) On the azimuthal mode structure of rotating blade flow instabilities axial turbomachines. AIAA Paper, A9630853. https://doi.org/10.2514/6.1996-1741
34. Li T, Wu Y, Ouyang H (2021) Numerical investigation of tip clearance effects on rotating instability of a low-speed compressor. Aerosp Sci Technol 111:106540. https://doi.org/10.1016/j.ast.2021.106540
35. Chen Z, Wu Y, An G (2021) Tip leakage flow, tip aerodynamic loading and rotating instability in a subsonic high-speed axial flow compressor rotor. Aerosp Sci Technol 110:106486. https://doi.org/10.1016/j.ast.2020.106486
36. Yue S, Wang Y, Wei L, et al. (2018) Experimental investigation of the unsteady tip clearance flow in a low-speed axial contra-rotating compressor, In: Proceedings of ASME Paper, Vol 2A, GT2018–76055
37. Patel P, Yang Y, Zha G (2020) Improved delayed detached eddy simulation (IDDES) of a 1.5 stage axial compressor non-synchronous vibration. Proceedings of ASME Turbo Expo 2020, GT2020–15073
38. He X, Ma H, Zhang J, Wei W (2013) Wavelet analysis of the shaft order perturbation and stall inception in an axial compressor. J Thermal Sci 22(3):223–228. https://doi.org/10.1007/s11630-013-0616-z
39. Wang H (2009) Experimental and numerical research of highly loaded axial-flow compressor stages, Beihang University, Doctoral dissertation
40. Liu B, Yu X, Liu H (2006) Application of SPIV in turbomachinery. Exper Fluid 40:621–642
41. Wu JZ, Ma H, Zhou M (2005) Vorticity and vortex dynamics. Springer, Berlin